Optics Letters

Low-power DAC-less PAM-4 transmitter using a cascaded microring modulator

RAPHAËL DUBÉ-DEMERS, SOPHIE LAROCHELLE, AND WEI SHI*

Department of Electrical and Computer Engineering, Centre d'optique photonique et laser (COPL), Université Laval, Québec, Canada
**Corresponding author: wei.shi@gel.ulaval.ca*

Received 31 August 2016; revised 20 October 2016; accepted 22 October 2016; posted 25 October 2016 (Doc. ID 274683); published 15 November 2016

Future super-computer interconnect systems and data centers request ultrahigh data rate links at low cost and power consumption, for which transmitters with a high level of integration and spectral efficient formats are key components. We report 60 Gb/s pulse-amplitude modulation (PAM-4) of an optical signal using a dual-microring silicon photonics circuit, making a low-power, digital-to-analog converter (DAC)-less PAM modulator. The power consumption is evaluated below 100 fJ/bit, including thermal adjustments. To the best of our knowledge, these results feature the lowest reported power consumption for PAM signaling in a DAC-less scheme for data rate beyond 40 Gb/s.

OCIS codes: (060.4510) Optical communications; (230.4110) Modulators; (130.0130) Integrated optics; (230.5750) Resonators.

http://dx.doi.org/10.1364/OL.41.005369

Due to the rapid growth of cloud services and global Internet usage, there is an increasing need for faster and cheaper optical interconnects. Silicon photonics (SiP) is a disruptive technology quickly emerging in answer to this need. Compatible to the proven complementary metal-oxide semiconductor fabrication process, it enables mass production and an unprecedented level of integration. Although widely examined, SiP interconnect transmitters remain an active research topic with few standards and consensus.

Most of the development of SiP modulators have traditionally been based on Mach–Zehnder interferometers (MZIs) [1,2] and microrings (MRMs) [3,4], with the notable exception of Bragg grating-based modulators [5]. Recently, the focus has changed to include complex modulation formats, known for their higher spectral efficiency [6,7]. Demonstrations of pulse-amplitude modulation (PAM) for direct detection systems have been presented using MZIs beyond 100 Gb/s [1,2] and using MRMs up to 80 Gb/s [3,8]. In order to reduce the cost, complexity, and power consumption of the modulators, electro-optic DAC-less schemes implemented using MZIs have been reported [9]. Additionally, the community developing the next generation of optical networks is increasingly making use of digital-signal processing (DSP) to further increase the data rate [7]. MRMs have also been used to generate a coherent modulation format up to 56 Gb/s [10], and are recognized as a potential solution for interchip links [11].

In this Letter, we report the operation of cascaded MRMs as an on-chip electro-optic modulator able to generate PAM-4 signal up to 60 Gb/s consuming below 100 fJ/bit. To our best knowledge, this result represents the fastest and lowest power optical modulator operating beyond 40 Gb/s in a DAC-less scheme. Further, since an all-electrical DAC also consumes power, this result possibly represents, in general, the fastest and lowest power optical PAM apparatus operating beyond 40 Gb/s.

We first describe the device and then report its static performances, i.e., under direct current (DC) excitation. We then proceed to the dynamical evaluation of the modulator, including large-signal bandwidth and bit error rate (BER) measurements. Finally, we evaluate the power consumption required for both the modulation and the thermal tuning of the modulator.

Multi-level signal generation is achieved by modulating independently two MRMs with uncorrelated pseudo-random binary sequences (PRBS). These two MRMs are coupled in series to the same bus waveguide in an all-pass configuration, as shown in Fig. 1(a). The layouts of both MRMs are identical and have been designed and optimized using the methodology found in [12]. In that sense, they exhibit the same transfer function, i.e., $T_1(V(t),\lambda) = T_2(V(t),\lambda)$, considering equal applied bias $V(t)$ and wavelength λ. However, due to fabrication errors, the response of each MRM will slightly differ. Therefore, the response of the modulator $T_{AC}(V(t),\lambda)$ must be taken as the product of the transfer function of each MRM, i.e., $T_{AC} \equiv E_{\text{out}}/E_{\text{in}} = T_1 * T_2$, as per Fig. 1(a), where the transfer function is defined as the ratio of the output electrical field E_{out} over the input electrical field E_{in}.

Each MRM makes use of the plasma dispersion effect through carrier depletion in a lateral *p-n* junction, as per Fig. 1(b). Strip and rib waveguides are implemented on a 220 nm thick silicon-on-insulator wafer where a 90 nm thick slab is used to implement rib waveguides, dopants, and electrical connections. The MRM has a coupling gap of 300 nm and a radius of 10 μm. The *p-n* junction mask boundary is centered with respect to the rib waveguide and the heavily doped regions are located 1 μm from the center of the rib waveguide whereas the medium doped regions are located 500 nm from the center.

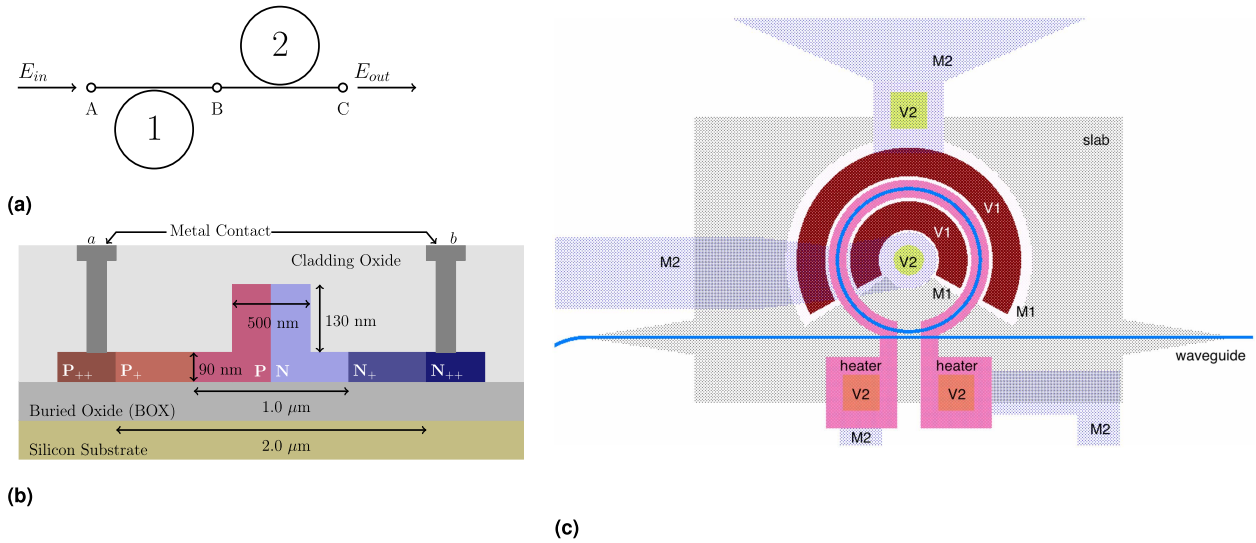

Fig. 1. (a) Schematic of the cascaded MRMs. (b) Cross section of the *p-n* junction showing relevant dimensions. Various metal layers are not representative of the actual layout. The heater layer is absent. (c) Layout of a single MRM showing the various metal layers (M1, M2), including the heaters and vias (V1, V2).

The design also contains a metal-based heater to compensate for wavelength fluctuations and fabrication errors [13], as shown in the partial mask layout of Fig. 1(c). The *p-n* junction spans roughly 70% of the circumference whereas the heater spans roughly 95% of the circumference. Optical in/out (I/O) is achieved via two etched surface grating couplers (SGCs) for transverse-electric polarized light. The modulator was fabricated through a dedicated run at IME A*STAR, Singapore, using deep UV lithography and phase-shifted mask technology.

One of the premises for the operation of this modulator is that the resonances of each MRM are aligned together so that they can efficiently modulate the same wavelength. This is a consequence of the channelized nature of MRMs. However, as shown in Fig. 2(a), due to fabrication errors, the resonances are not initially aligned. The positive thermo-optic coefficient of silicon results in a redshift of the resonance when the temperature of the waveguide increases. Hence, heating one MRM allows one to compensate for the process variations and align the resonances. In addition, the measured extinction ratio (ER) becomes greater than 30 dB under alignment.

Another premise for this modulator is that each MRM is fed by a PRBS. One possibility would be to slightly offset the individual resonances so that, for a given wavelength and voltage swing, each MRM would produce a different optical modulation amplitude (OMA); one would then act as the most significant bit (MSB) and the other as the least significant bit (LSB). The other possibility is to align the resonances and drive the MRMs using two different voltage amplitudes. In this Letter, we use the latter method to avoid distortion. Indeed, the pulse shape being a direct function of the frequency detuning [12], operating the MRMs at different detuning would mean that the two resonators would exhibit different time responses and thus, introduce distortion.

Figure 2(b) shows the results of our simulations using the model of [12] and illustrates the behavior of the modulator. In particular, it shows that the OMAs add up but that the

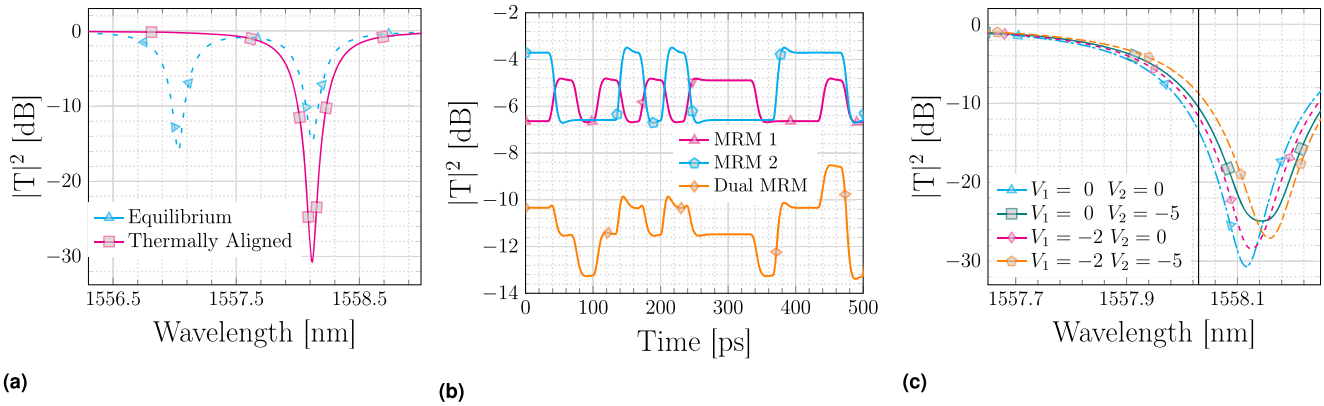

Fig. 2. (a) Measured spectra showing the position of the resonances as fabricated (equilibrium) and after tuning (thermally aligned), respectively. (b) Simulated transmission of each MRM and the corresponding transmitted power of the cascaded system. (c) Measured transmission spectra illustrating the four different states used in the PAM-4 demonstration. The vertical line shows the position of the laser used. The operating wavelength λ is 1558.028 nm. Note that the measured spectra in (a) and (c) are normalized to the SGC response.

insertion losses also add up, as reported in other demonstrations using cascaded MRMs [14]. Moreover, it shows how two MRMs with aligned resonances produce a four-level signal from two PRBSs of different amplitudes. Figure 2(c) shows the measured spectra of the modulator when the resonances are aligned. The four states needed to produce the PAM-4 signal are well visible. From these measurements, we extract the efficiency of the MRM, which is found to be roughly 1 GHz/V. The free spectral range is 9.78 nm and the quality factor Q is roughly 5200 for each MRM under equilibrium.

We use a BER test system that includes two sources to produce two uncorrelated PRBSs of $2^{15} - 1$ bits and a clock. Radio frequency (RF) delay lines are used on each channel to synchronize both signals. The synchronization process is paramount since it takes care of the differential delay between the electrical lines and of the optical delay between each MRM. The signals are then amplified using 55 GHz RF amplifiers and biased using 70 GHz bias tees. Hence, the two PRBSs having an initial amplitude of 450 mV are amplified to 5 V and 2 V, respectively. One can note that the amplitude used for the LSB is less than half of the MSB, because of the non-linearity of the transfer function of the MRM [3]. We then use a GSGSG (Ground-Signal) configured, 50 Ω terminated, 50 GHz micro-probe to feed the electrical signals on-chip. In addition to the RF probe, a DC probe, in conjunction with a DC source are used to control the MRM heaters. A picture of the fabricated device is available in [15], including the pads layout.

The optical portion of the test setup consists of a tunable laser used as the optical source, a polarization-maintaining fiber, and a 250 μm spaced fiber array, aligned over the SGCs. The modulated light is collected and then amplified using an erbium-doped fiber amplifier (EDFA). The amplified spontaneous emission coming from the EDFA is filtered out using a tunable optical filter. Before the photo-detector, a variable attenuator and power meter is used to control and monitor the power of the received signal. Finally, the 70 GHz photo-detector operates the optical to electrical conversion. The electrical signal is then captured using a 160 GSample/s, 63 GHz real-time oscilloscope. A computer is used to perform off-line DSP. The DSP procedure includes filtering, resampling, and equalization of the signal using a minimum mean square error (MMSE) filter. The BER measurements presented in this Letter have been obtained using the DSP procedure described in [3] using 30 taps and 2000 training symbols in the implementation of the MMSE filter. Moreover, the BER values are counted on a minimum of 4 million symbols.

Figure 3 presents examples of measured eye diagrams and BER. Figures 3(a) and 3(c) present examples of optical eye diagrams taken right before the photo-detector, whereas Figs. 3(b) and 3(d) provide eye diagrams after the DSP procedure. We underline that, since we apply the MMSE filter on sequences that have been downsampled to one sample per bit, we use an anti-aliasing filter and upsampling of the signal in order to produce the eyes of Figs. 3(b) and 3(d). This procedure is also described in [3]. Figure 3(e) provides the counted BER, thus proving the concept of the optical DAC based on MRMs up to 60 Gb/s while maintaining figures under the FEC threshold. Finally, using a single MRM, we measured the large-signal bandwidth to roughly 25 GHz, that is, the frequency at which the eye loses 3 dB in its dynamical ER.

The aim of the current demonstration is to show the feasibility of generating a PAM signal on-chip using the lowest amount of power. To that extent, two different contributions must be considered, the power consumed in the modulation, i.e., charging the capacitance of the p-n junction, and the power consumed by the heater to maintain the MRMs aligned.

The capacitance of the p-n junction is calculated to 6.2 fF using the model found in [12]. Thus, using the product of the

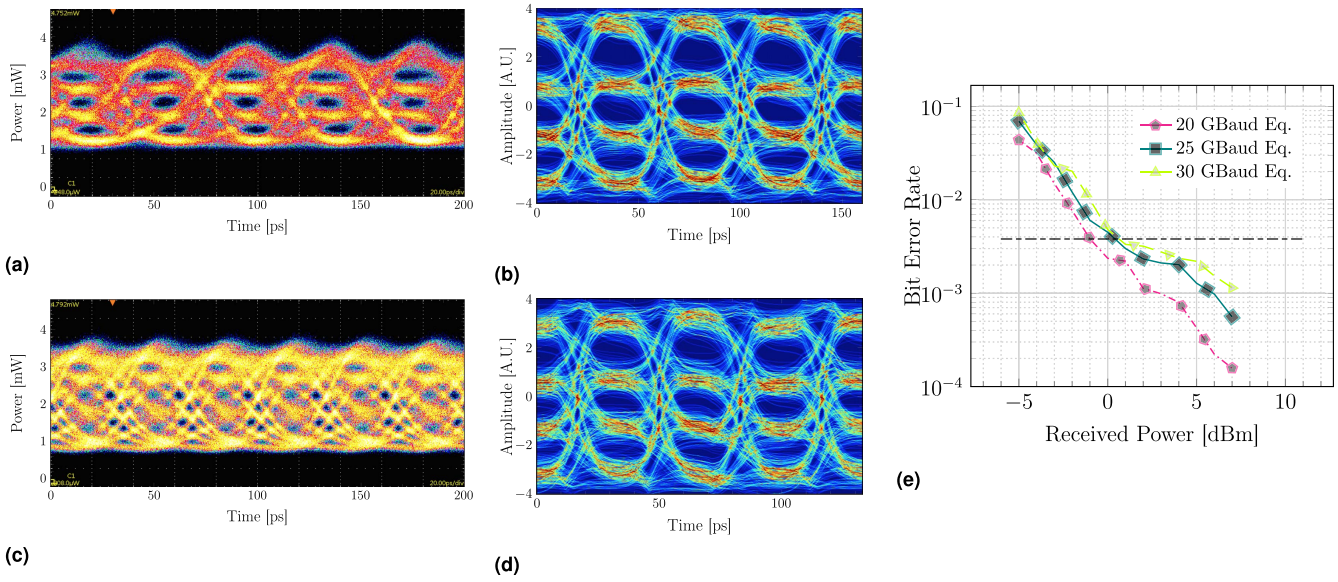

Fig. 3. (a, c) Measured optical eye diagrams at 25 GBaud (50 Gb/s) and 30 GBaud (60 Gb/s), respectively. The received power in both figures is around 5 dBm. (b, d) Equalized eye diagrams at 25 GBaud and 30 GBaud, respectively. The received power in both figures is 7 dBm. (e) BER measurements after a 30 taps MMSE equalizer. The horizontal line indicates the $3.8 \cdot 10^{-3}$ pre-forward error correction code (FEC) threshold for error-free transmission, i.e., $<10^{-15}$, when suffering a 6.7% overhead [16].

capacitance C by the square of the driving voltage V, one can estimate the energy consumed by the charging diode E_{pn}, i.e., $E_{pn} = CV^2$. In this case, we find out that the LSB consumes 6 fJ/bit and the MSB consumes 39 fJ/bit, for a total of 45 fJ/bit when doing PAM-4.

Further, compared to other technologies, the modulation efficiency of this modulator is rather low. In fact, using multi-project wafer services of commercial foundries, a value of 2 GHz/V has been reported for a lateral p-n junction [3]. For example, reducing the slab thickness could increase the optical mode confinement, thereby increasing light–matter interactions and reducing the power consumption.

The efficiency of the heater is measured at 23 μW/GHz, which advantageously compares to typical results [3]. However, custom processes combined with smaller resonant modulators have yielded tuning efficiency up to 3 times higher than the present demonstration [17]. Nevertheless, roughly 3 mW of heating power are needed to maintain the state of the modulator, which results in a power consumption of 50 fJ/bit around 60 Gb/s.

Accordingly, the total power consumption of the modulator here presented is in the vicinity of 100 fJ/bit for data rates of 50–60 Gb/s, which is quite low considering that this power budget includes the DAC. In fact, it is advantageously comparable to a similar demonstration using an MZI [18], in which the use of segmented electrodes allows the generation of a PAM signal, but at a much higher power consumption, i.e., 7.7 pJ/bit. Nonetheless, one must consider that this dramatic reduction in power consumption at the transmitter side results in a trade-off, the degradation of the performances at the receiver side. For instance, compared with [18], our results show around 8 dB of power penalty at 20 GBaud for a BER of 10^{-3}.

Also, it is reported that a single MRM, driven by an external DAC, can operate in the vicinity of 10 fJ/bit [3], when considering the sole power consumption of the MRM. In that latter case, the power penalty is around 3 dB, when compared to our results. Unfortunately, the picture is incomplete since the power used by the DAC is unknown. Thus, it appears that additional considerations are needed in order to determine which method would perform better under given circumstances.

We have demonstrated the generation of PAM-4 signal using a dual MRM system operating without the need for an electrical DAC. We have proved our concept up to 60 Gb/s and shown that the modulator uses less than 100 fJ/bit at this data rate, including the thermal tuning of the modulator. Consequently, this demonstration is, to the best of our knowledge, the lowest power used in an all-optical PAM generation and transmission beyond 40 Gb/s. Improved performances are expected as the design is optimized and more degrees of freedom used. Further reduction in the power consumption is also expected as the fabrication variations are reduced. Refinement of the DSP procedure might yield higher data rate and/or lower power consumption as the driving voltage might be reduced. These results are encouraging for the elaboration of low-power, low-cost optical interconnects for next-generation systems.

Funding. Natural Sciences and Engineering Research Council of Canada (NSERC) (RDCPJ438811-12); PROMPT (PJT-2011-17); Ciena; Fonds de Recherche du Québec-Nature et Technologies (FRQNT) (2016- NC-190737).

Acknowledgment. This work is part of the SPEED research project (Silicon Photonic Electrically Engineered Devices) funded by NSERC, PROMPT, and Ciena. We also acknowledge the contribution and technical support of CMC Microsystems.

REFERENCES

1. A. Samani, M. Chagnon, D. Patel, V. Veerasubramanian, S. Ghosh, M. Osman, Q. Zhong, and D. V. Plant, IEEE Photon. J. **7**, 1 (2015).
2. M. Chagnon, M. Osman, M. Poulin, C. Latrasse, J.-F. Gagné, Y. Painchaud, C. Paquet, S. Lessard, and D. V. Plant, Opt. Express **22**, 21018 (2014).
3. R. Dubé-Demers, S. LaRochelle, and W. Shi, Optica **3**, 622 (2016).
4. J. Müller, F. Merget, S. Sharif Azadeh, J. Hauck, S. Romeo García, B. Shen, and J. Witzens, Sci. Rep. **4**, 6310 (2014).
5. K. Bédard, A. D. Simard, B. Fillion, Y. Painchaud, L. A. Rusch, and S. LaRochelle, Opt. Express **24**, 2413 (2016).
6. C. Cole, I. Lyubomirsky, A. Ghiasi, and V. Telang, IEEE Commun. Mag. **51**(3), 50 (2013).
7. Y. Kai, M. Nishihara, T. Tanaka, and T. Drenski, in *European Conference on Optical Communications (ECOC)* (2013), paper Th1F3.
8. L. Wang, R. Hu, L. M. Feng, Y. Qui, X. Xiao, D. Chen, Q. Yang, S. Yu, Z. Li, J. Yu, and Y. Yu, in *Asia Communications and Photonics Conference (ACPC)* (2014), paper ATh4D.
9. D. Patel, A. Samani, V. Veerasubramanian, S. Ghosh, and D. V. Plant, IEEE Photon. Technol. Lett. **27**, 2433 (2015).
10. P. Dong, C. Xie, L. L. Buhl, and Y.-K. Chen, in *Optical Fiber Communication Conference (OFC)* (2013), paper OW4J.2.
11. G. Li, A. V. Krishnamoorthy, I. Shubin, J. Yao, Y. Luo, H. Thacker, X. Zheng, K. Raj, and J. E. Cunningham, IEEE J. Sel. Top. Quantum Electron. **19**, 3401819 (2013).
12. R. Dubé-Demers, J. St-Yves, A. Bois, Q. Zhong, M. Caverley, Y. Wang, L. Chrostowski, S. LaRochelle, D. V. Plant, and W. Shi, J. Lightwave Technol. **33**, 4240 (2015).
13. P. Dong, R. Shafiia, S. Liao, H. Liang, N.-N. Feng, D. Feng, G. Li, X. Zheng, A. V. Krishnamoorthy, and M. Asghari, Opt. Express **18**, 10941 (2010).
14. T. Gu, Y.-K. Chen, C. W. Wong, and P. Dong, Opt. Lett. **39**, 4974 (2014).
15. R. Dubé-Demers, S. LaRochelle, and W. Shi, in *IEEE Optical Interconnects Conference (OI)* (2016), pp. 28–29.
16. "Media access control parameters, physical layers, and management parameters for 40-Gb/s and 100-Gb/s operation," IEEE Std. 802.3ba (2010).
17. W. A. Zortman, A. L. Lentine, D. C. Trotter, and M. R. Watts, in *Optical Fiber Communication Conference (OFC)* (2012), paper OW4I.5.
18. A. D. Simard, B. Filion, D. Patel, D. Plant, and S. LaRochelle, Opt. Express **24**, 19467 (2016).